Journal of Applied Polymer Science

# Microstructure-Based Fatigue Modeling of an Acrylonitrile Butadiene Styrene (ABS) Copolymer

**Marcos Lugo,[1] Jason E. Fountain,[1] Justin M. Hughes,[1] Jean-Luc Bouvard,[1,2] Mark F. Horstemeyer[1,3]**

[1]Center for Advanced Vehicular System, Mississippi State University, Starkville, Mississippi 39759
[2]Mines-ParisTech, CEMEF, UMR 7635, BP 207, 06904 Sophia Antipolis cedex, France
[3]Department of Mechanical Engineering, Mississippi State University, Starkville, Mississippi 39759
Correspondence to: M. Lugo (E-mail: marcos@cavs.msstate.edu)

**ABSTRACT:** In this article, we experimentally investigate the structure–property relationships of an acrylonitrile butadiene styrene (ABS) copolymer for fatigue and use a microstructure-based multistage fatigue (MSF) model to predict material failure. The MSF model comprises three stages of fatigue damage (crack incubation, small crack growth, and long crack growth) that was originally used for metal alloys. This study shows for the first time that the MSF theory is general enough to apply to polymer systems like ABS. The experimental study included monotonic testing (compression and tension) and fully reversed uniaxial cyclic tests at two frequencies (1 Hz and 10 Hz) with a range of strain amplitudes of 0.006 to 0.04. Cyclical softening was observed in the ABS copolymer. Fractography studies of failed specimens revealed that particles were responsible for crack incubation. Although polymeric materials can be argued to be more complex in terms of failure modes and thermo-mechano-chemical sensitivity when compared with most metal alloys, results showed that the MSF model could be extended successfully to capture microstructural effects to polymeric materials. © 2014 Wiley Periodicals, Inc. J. Appl. Polym. Sci. **2014**, *131*, 40882.

**KEYWORDS:** mechanical properties; properties and characterization; structure–property relations; theory and modeling; thermoplastics

Received 5 February 2014; accepted 23 April 2014
**DOI: 10.1002/app.40882**

## INTRODUCTION

Energy efficient design, particularly for automotive components using lightweight materials such as metal alloys and polymers, has become of great interest in the last decade in order to reduce emissions and increase gas mileage. This heightened interest has encouraged further investigations into polymers within the materials science community for their ability to achieve targeted strength and elongation properties, and maybe more importantly, impact and fatigue resistance. The increase in the application of polymeric materials for automotive structural and exterior components continues to grow, correspondingly magnifying the need for models capable of producing highly reliable fatigue predictions. Furthermore, the long-term reliability of polymers in fatigue is currently not well understood, and consequently, modeling of polymer fatigue is lacking in literature.

The material subject of investigation in this work is a thermoplastic and a copolymer (acrylonitrile butadiene styrene (ABS)) which is classified also as a glassy polymer for temperature below its glass transition temperature ($T_g = 105°C$). Microstructure of polymer differs significantly from metals. While metals are crystallographic organized structure, most of polymers are composed by long chains of atoms and a few of them have semi-crystalline structure; however, the crystallographic planes are not formed as in metals. Despite the noticeable differences, polymers also fail due to fatigue damage much like metallic materials fail, initiating at high stress concentrations within the material due to microstructural heterogeneities. For glassy thermoplastics, these heterogeneities include impurities, additives, and defects found within the material.

It has been widely established that the lifetime of metallic materials can be determined by means of a stress-life (S-N), strain-life ($\varepsilon$-N), or fracture mechanics approaches. These approaches have been also used for polymers by many researchers.[1,2] In the early 1970s, Rabinowitz et al.[1] investigated the fatigue behavior of Polystyrene, a glassy polymer. The stress or strain range and mean stress parameters were found to have a major influence on the lifetime of polymers, similar to metals. Three regions were identified for the stress-life curve shown in Figure 1. Region (I) is a quasi-plateau zone common to many thermoplastics at high stress amplitudes. Region (II) is an intermediate zone of linear

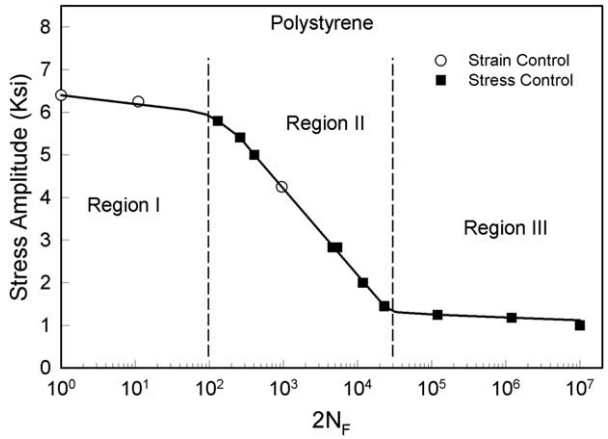


**Figure 1.** Stress-life curve for Polysterene[1] illustrating the three regions of a polymer fatigue process.

behavior. Finally, Region (III) is the long-life region similar to the fatigue endurance observed for metals. In addition, the cyclic stress response was discussed in terms of stress evolution.[1,2] In the stress evolution curve (stress amplitude versus number of cycles), they distinguished four regimes for the cyclic stress–strain response of thermoplastics: incubation, transition, cyclic stability, and crack propagation. After the monotonic response of the first cycle, an incubation period followed featuring a cycling softening. The incubation period or delay time is an early of deformation process where localization of stresses is formed at compositional defects, flaws, and inclusions. The transition region is characterized by a rapid change in the peak stress. In this region, thermal contributions are not identified, and proceeding in symmetrically manner implying that not crack propagation is involved. The cyclic stability region constitutes most of the fatigue life of thermoplastic material and at the end of this stage the crack starts. The last region was identified by a cyclical decrease in the peak tensile stresses and an approximately constant compressive stress which are typical of crack propagation. These stages observed for the stress evolution behavior of the thermoplastic are very useful in providing understanding for the fatigue damage model. However, the Rabinowitz et al.[2] description is not a quantification of the multiple stages of the fatigue process. Therefore, it is still needed to find a form of evaluating quantitatively the damage on every stage. Moreover, despite of the interest in polymeric materials at present time, the literature regarding the stress-life and strain-life for polymers is not as vast as for metals.

A major assumption of fracture mechanics approach is that material is initially flawed; therefore, the initial stages of fatigue damage are neglected. Furthermore, for polymers the crack propagation stage is believed to last significantly more than the crack nucleation as suggested by Radon.[3] This point of view has prevailed to date as corroborated by the large number of papers addressed using fracture mechanics methods. Nonetheless, fracture mechanics has allowed the study of the micromechanisms of failure in polymers.[3–9] Studies on the micromechanisms of glassy polymers showed that there are two primary types of failure mechanisms and crack growth: normal fatigue crack propagation and retarded fatigue crack propagation.[3,5,7,10] In the normal type, the material is fibrillated to form a craze at the same speed that fibrils are broken in front of the crack tip; hence, the crack propagates with almost a constant craze length. On the other hand, retarded fatigue crack propagation can occur because of a crazed region before any crack advancement.[3,5,7,10] Although the current body of literature is abundant on these two primary competing failure mechanisms, the mechanisms are still not completely well understood. As discussed above, this method does not consider early stages of fatigue damage. However, Chen et al.[11] have found for glassy polymers that 2/3 of total life is spent before start to craze. Consequently, microstructure-based fatigue modeling of thermoplastic polymers is also lacking in literature.


**Figure 2.** An acrylonitrile butadiene styrene (ABS) copolymer cylindrical dog-bone shaped fatigue specimen mounted in an MTS 810 servo-hydraulic load frame with an MTS model 634.31F-25 axial extensometer for strain-control testing and an Optris Laser thermometer for monitoring temperature generation. [Color figure can be viewed in the online issue, which is available at wileyonlinelibrary.com.]

The purpose of this study was to experimentally quantify the fatigue behavior and the structure–property relationships of an ABS copolymer and then correlate experimental data to a microstructure-sensitive model to capture fatigue behavior. The incorporation of the microstructural characteristics of metal alloys and polymers through a microstructural-based model using a multistage fatigue (MSF) model is a step toward more closely aligning the fracture analysis of polymers and metals. The MSF model, originally developed for aluminum alloys by McDowell et al.,[12] has the capability to capture the microstructure effects and reflects three regimes of crack growth[13]: crack incubation (INC), microstructurally small crack or physically small crack (MSC), and long crack (LC), for both low cycle fatigue (LCF) and high cycle fatigue (HCF). Fully reversed uniaxial strain life experiments and observations were performed to experimentally and computationally quantify fatigue structure–property relationships. Optical microscopy and scanning electron microscopy (SEM) of fatigue fracture surfaces was used to quantify the microstructural properties.

## EXPERIMENTAL

The material used in this study is an engineering grade, high impact thermoplastic ABS copolymer, which is beige in color

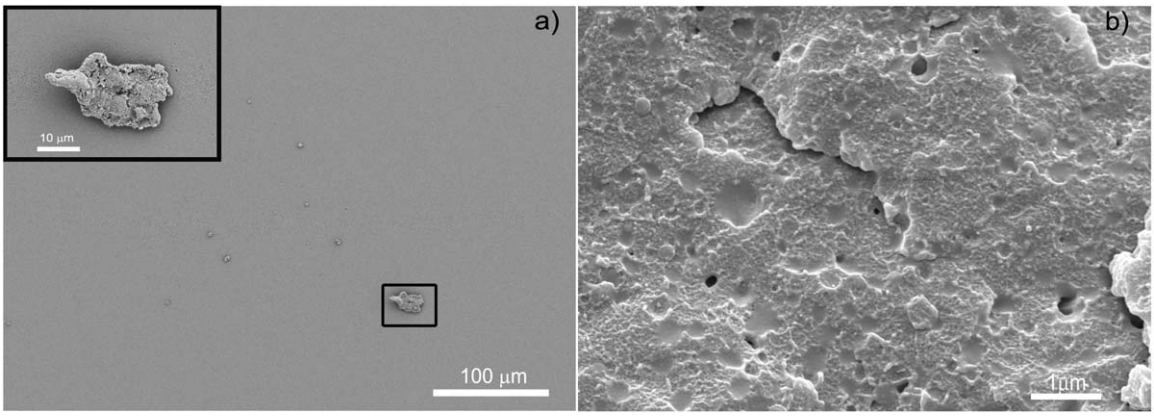


**Figure 3.** Microstructure of acrylonitrile butadiene styrene copolymer (ABS): (a) particles and (b) pores.

and produced by King Plastic Corporation. The nominal compositions chosen for the synthesis of the commercially available ABS are the following: acrylonitrile 20–30%, butadiene 5–35%, and styrene 35–75%. The material used in this study was supplied in the form of a plate with dimensions of 25 × 610 × 610 mm.

### Monotonic Loading

Monotonic tensile and compression experiments were performed using an Instron 8850 load frame. An INSTRON 2630-110 extensometer was used and a feedback loop between the extensometer and the load frame was used to ensure a constant engineering strain rate over the entire duration of each test. Tensile specimens following ASTM D638-03 standard were designed.

Cylindrical specimens with a diameter of 12.7 mm and a length of 6.35 mm were used for compression tests. This geometric configuration has been used for thermoplastic polyurethane by Zaroulis and Boyce.[14] Two types of moly-paste lubricants supplied were used on the compression specimens and compression platens to minimize friction and to prevent specimen barreling.

### Fatigue Experiments

Completely reversed fatigue experiments were conducted over a range of strain amplitudes (0.005–0.05) at two frequencies (1 Hz and 10 Hz) to capture the low cycle regime of an ABS copolymer. The tests were performed using an MTS 810 servo-hydraulic load frame, as shown in Figure 2, in an ambient laboratory environment. An MTS model 634.31F-25 axial extensometer was used for strain controlled tests. A cylindrical dog-bone shaped specimen was designed based on the ASTM E 606-04 standard. The specimens were tested until failure and temperature generation was monitored using an Optris laser thermometer.

**Table I.** Particle and Porosity Properties Obtained Through Image Analysis of the Virgin Microstructure of an Acrylonitrile Butadiene Styrene Copolymer

| Average particle diameter ($\mu$m) | Average nearest neighbor ($\mu$m) | Average pore size ($\mu$m) | Pore nearest neighbor ($\mu$m) | Porosity (%) |
|---|---|---|---|---|
| 3.55 | 1.37 | 0.059 | 0.186 | 3.62 |

### Fractography

Fracture surfaces of the fatigued specimens were obtained by first cutting the failed specimens and then sputter coated for SEM observation. Surfaces were first examined using an optical microscope to obtain an overall fracture surface map. In addition, virgin specimens were cut from the as-received material and were ultrasonified for 15 min to remove any impurities,

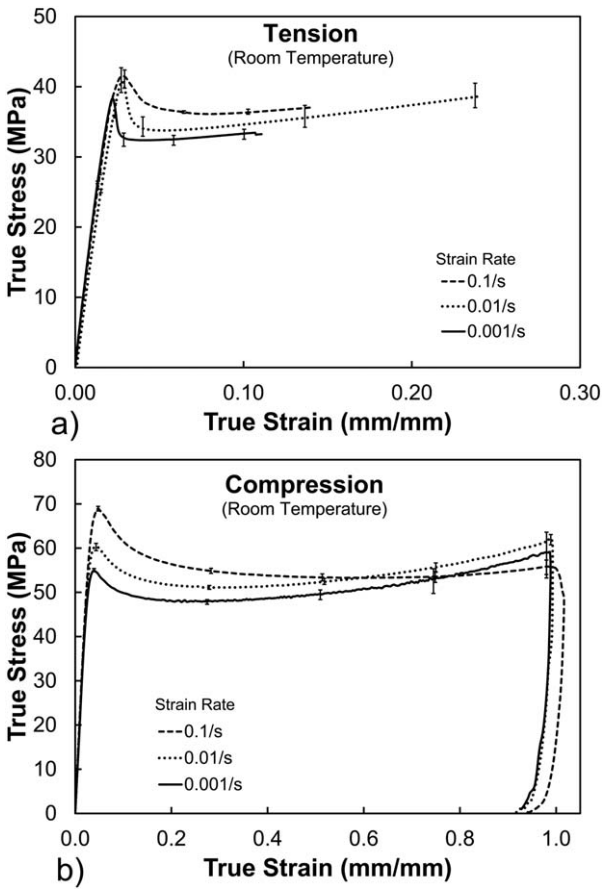


**Figure 4.** Monotonic stress–strain plots of an acrylonitrile butadiene styrene (ABS) copolymer in (a) tension and (b) compression.

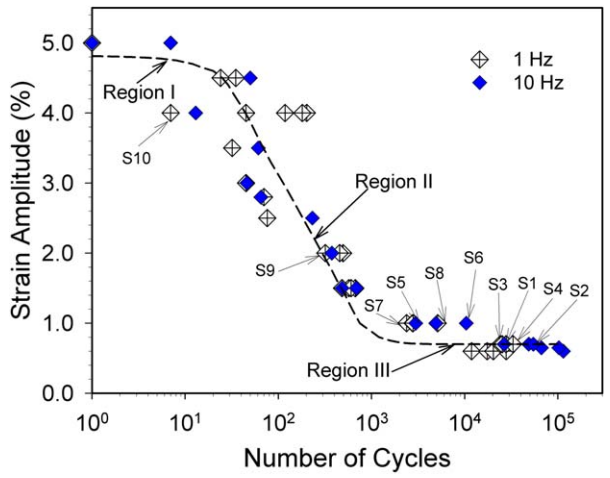


**Figure 5.** Acrylonitrile butadiene styrene (ABS) control fatigue life plot for cylindrical dog bone fatigue specimens tested at 1 Hz and 10 Hz. Note: A run-out specimen was fatigued at 10 Hz at a strain amplitude of 0.005 for over 10 million cycles. [Color figure can be viewed in the online issue, which is available at wileyonlinelibrary.com.]

followed by polishing process, and SEM to determine the microporosity for the virgin ABS copolymer specimens. SEM was also used to determine the initiating particle for the fatigue crack.

## RESULTS AND DISCUSSION

### Microstructure

Microstructural features were determined from optical micrographs of the virgin ABS copolymer as shown in Figure 3. Results of the digital image analyses are summarized in Table I. Second phase particles and porosity were observed within the matrix as observed in Figure 3. Large inclusions ranging from around 60 $\mu$m to ~81 $\mu$m were found, and EDS analyses of defects or inclusions revealed that the primary composition was polybutadiene due to the high percentage of carbon with trace amounts of nitrogen that can be attributed to small amounts of acrylonitrile. Regarding the inclusion particles present in the material, the particles had an average particle size of 3.55 $\mu$m.

### Monotonic Loading

The effect of strain rate on the mechanical behavior of the ABS copolymer in tension and compression is given in Figure 4, which shows the true stress−true strain response in an ambient laboratory environment at 25°C with engineering strain rates of 0.001/s, 0.01/s, and 0.1/s. Monotonic, tension, and compression test data were averaged and plotted with their respective error bars for all strain rates. The stress response in tension shows the typical increase in the yield and peak stresses and a general flattening of the subsequent softening as strain increases, which can be attributed to necking. The stress response in compression exhibits three regimes as noted in Figure 4(b) for compression:

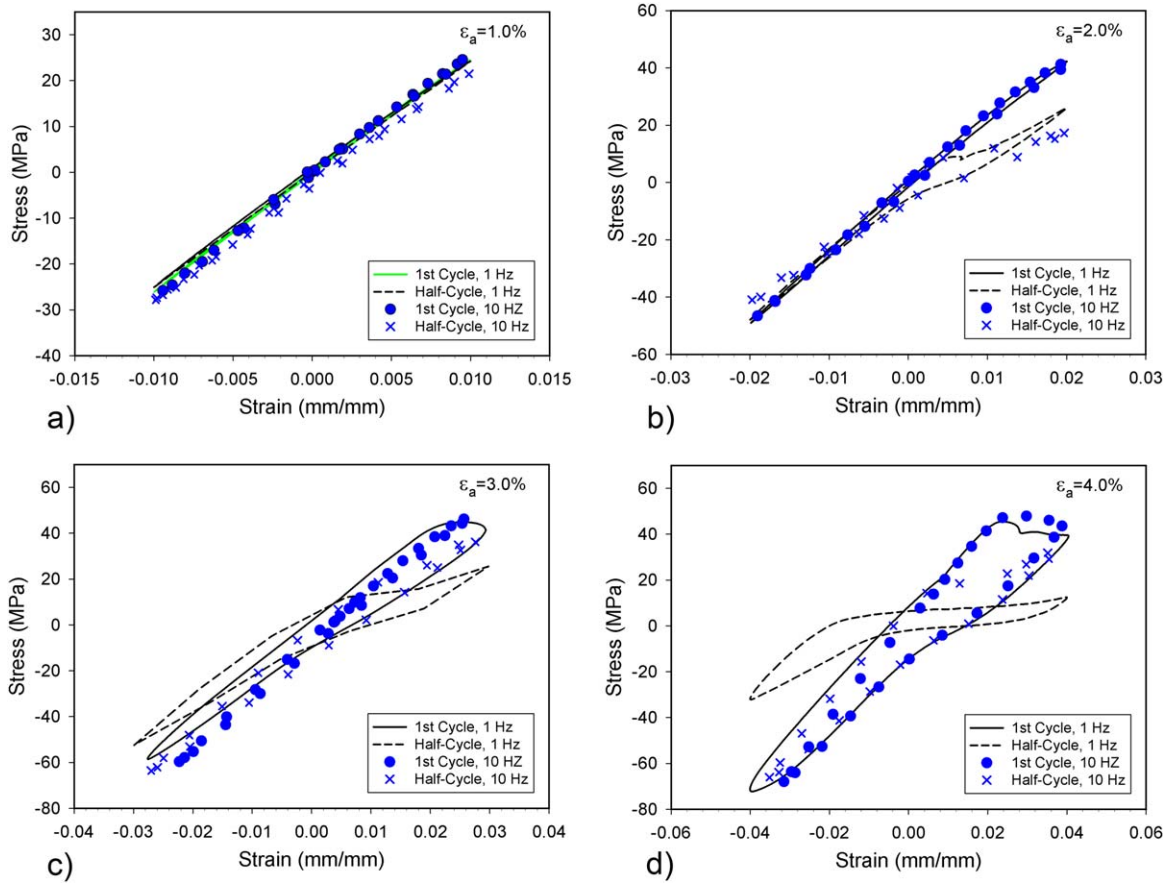


**Figure 6.** First cycle and half-life cycle hysteresis loops for an ABS copolymer tested at 1 Hz and 10 Hz with applied strain amplitudes of (a) 0.01, (b) 0.02, (c) 0.03, and (d) 0.04. [Color figure can be viewed in the online issue, which is available at wileyonlinelibrary.com.]

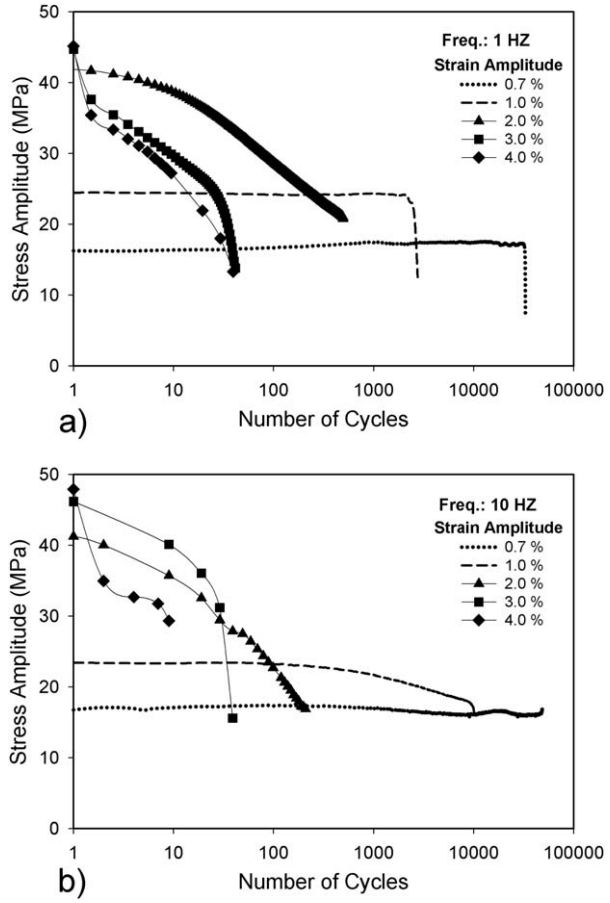


**Figure 7.** Peak tensile stress versus number of cycles to 50% load drop for increasing applied total strain amplitudes for ABS fatigue specimens performed at (a) 1 Hz and (b) 10 Hz.

an initial linear elastic response followed by a nonlinear transition curve to global yield, followed by strain softening attributed to chain rearrangement and subsequent strain hardening attributed to the alignment of these chains.

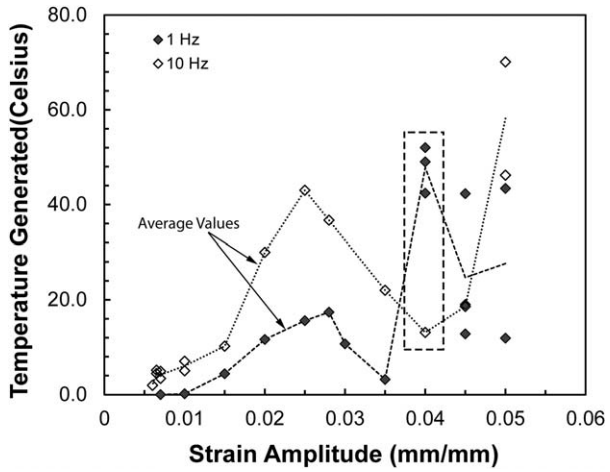


**Figure 8.** The temperature generation profile for initially ambient temperature acrylonitrile butadiene styrene (ABS) copolymer fatigue specimens tested at 1 Hz and 10 Hz at corresponding strain amplitudes.

### Strain-Life

Figure 5 shows the ABS strain-life curve exhibiting a pattern similar to that referred by Rabinowitz et al.[2] where three distinct regions are shown. Highlighted in this chart are some specific points that were subjected to further analysis as S1, S2, S3, etc., which are associated as follows: S1, sample 1; S2, sample 2; and so on. First, a plateau is observed for the first region (Region I) followed by a quasi linear section (Region II). This region comprises most of the strain-life curve. Finally, the long-life region can be observed, which illustrates the fatigue resistance of the material. Marissen et al.[15] observed that longer lifetimes arose for higher frequencies, which could partially be attributed to thermal softening for increased equivalent strain rates at 10 Hz.[16]

### Hysteresis and Stress Response

The initial and half-life hysteresis loops for ABS specimens are contrasted in Figure 6. A softening effect was observed for the entire range of strain amplitudes under investigation at both 1 Hz and 10 Hz frequencies. However, this effect is more pronounced at higher strain amplitudes. From the strain amplitude of 0.02, a broadening of the hysteresis loop begins to develop for specimens fatigued at both frequencies attributed to yielding of the ABS material. It is also observed that at higher strain levels the evolution of hysteresis loops were larger for frequencies of 1 Hz than for frequencies of 10 Hz. It can be attributed to the fact that an increase in the frequency results in an increase on the strain rate. Therefore, a higher strain rate will originate a higher modulus and yield strength.[17] The final effect on the stress–strain response can be that for lower frequencies such as 1 Hz more inelasticity is evident earlier than that for the 10 Hz frequency.

The evolution of stress amplitude as a function of number of cycles to 50% load drop for ABS is shown in Figure 7. These curves show the response of the material under fatigue loading and provide the path by which the material reaches final failure. Figure 6 demonstrates clearly that over the entire range of strange amplitudes the material behaves such as a ductile polymer which is featured by cyclic softening. It is due to a decrease in the material resistance to nonelastic strain with reversed deformation.[1,2] While this effect is present for all strain levels that was less significant for the lower strain amplitudes.

### Temperature Generation

The temperature of the specimen surface for strain control fatigue tests was monitored using an Optris laser thermometer for specimens fatigued at 1 Hz and 10 Hz over a range of strain amplitudes (0.007 to 0.05). The temperature generated at the surface for each fatigue specimen was plotted versus the corresponding strain amplitude as shown in Figure 8.

The temperature increased, decreased, and then increased again as the stress increased, decreased, and increased as the deformation proceeded. An increase in the temperature generated at the specimen surface during the fatigue tests was observed throughout the elastic regime to strains of ~0.025 for 1 Hz and 0.028 for 10 Hz, which corresponds to yielding of the ABS copolymer. Beyond yield, the temperature

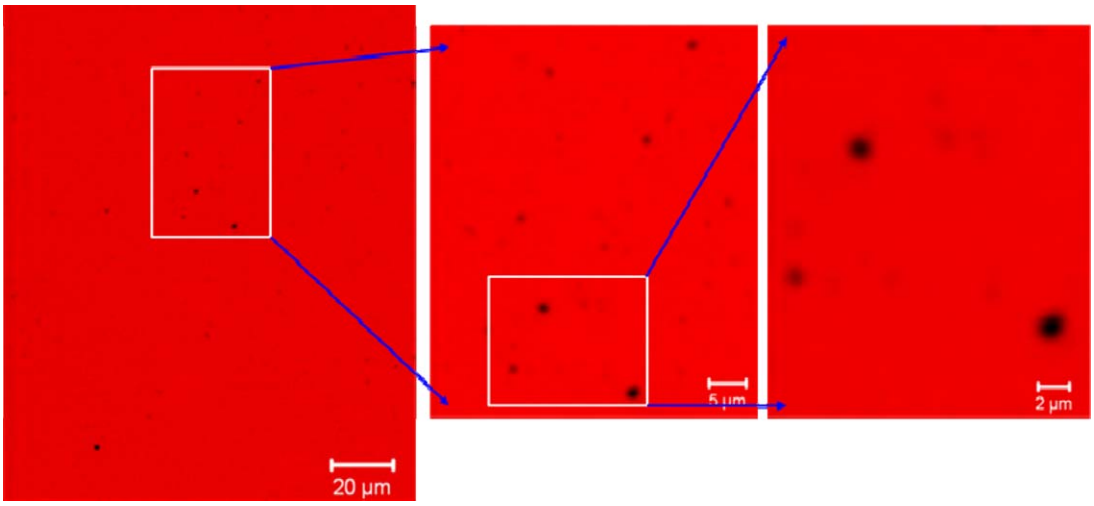


**Figure 9.** Optical micrographs of the sectioned ABS before testing, showing the presence of rubber particles (in black color) at three length scales. [Color figure can be viewed in the online issue, which is available at wileyonlinelibrary.com.]

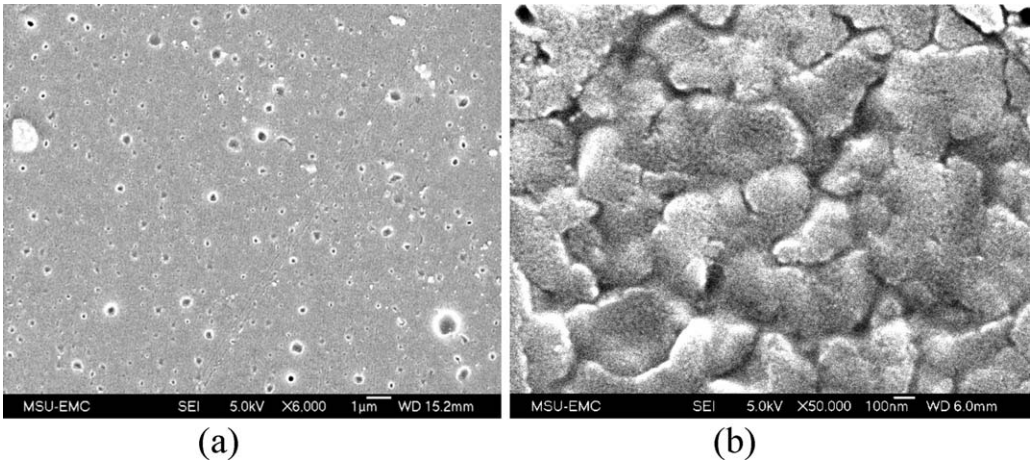


**Figure 10.** SEM images of phase structure of a commercial ABS grade: (a) an enlarged view of rubber displaying the particles, and (b) a zoomed-in view showing a single rubber particle.

decreased throughout the viscoplastic regime to 0.035 strain amplitude for 1 Hz and 0.04 strain amplitude for 10 Hz, respectively. The subsequent increase in temperature was observed throughout the deformation-induced hardening regime to failure.

The increase in temperature to yield could be attributed to the stretch and ordering of polymer chains. The polymer chains are aligned at yield and begin to inelastically stretch until ultimate failure.[18] The subsequent softening beyond yield has an associated temperature decrease. Furthermore, the final increase in

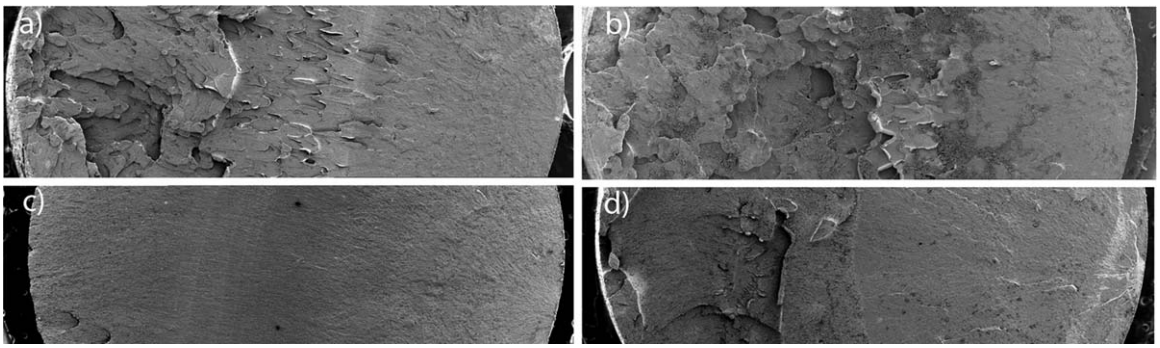


**Figure 11.** Fracture surface maps of acrylonitrile butadiene styrene (ABS) copolymer fatigue specimens designating the different regimes of crack growth for frequencies and strain amplitudes, respectively, of the following: (a) 1 Hz, 0.007, (b) 1 Hz, 0.01, (c) 10 Hz, 0.007, and (d) 10 Hz, 0.01.

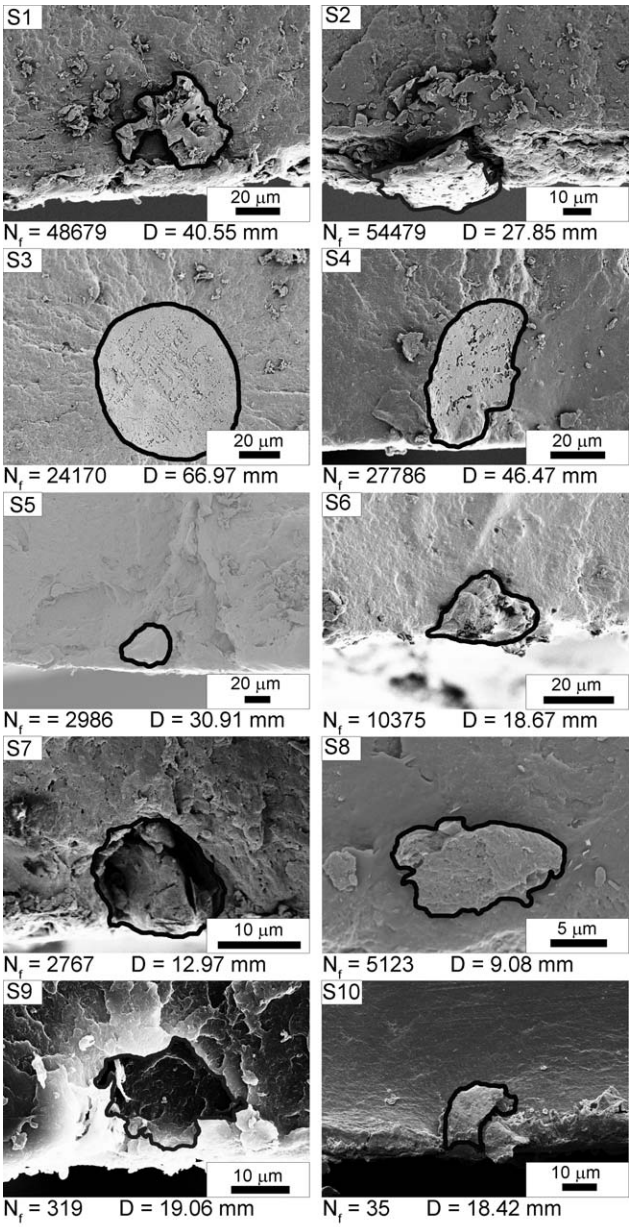


**Figure 12.** Scanning electron micrographs for particles responsible for incubating fatigue cracks for upper and lower bounds of fatigue life of acrylonitrile butadiene styrene (ABS) copolymer specimens, where $N_f$ is the number of cycles to failure, and $D$ is the square root particle area.

temperature during larger deformations could be attributed to the overall stretch, alignment, and final fracture of remaining long polymer chains. The temperatures generated for a frequency of 10 Hz were greater than that for a frequency of 1 Hz in the elastic regime and the post-yield softening regime; however, in the higher "hardening" regime at large deformations, because of the scatter it is hard to deduce which is greater. The transition occurs at strain amplitudes of about 0.04.

The evolving texture was not captured by the current MSF model for the ABS copolymer in this study, although the orientation effects can be captured. For metals, the texture effect was included via Taylor Factors, but for polymers those are not available. As such, the ability to capture evolving texture effects for polymers due to their higher sensitivity in processing and loading should be developed for the MSF model in future work.

**Fractography**

The strength and toughness of an amorphous glassy monophase (styrene acrylonitrile (SAN)) can be improved by the addition of a second noncontinuous phase (rubber particles).[19,20] A typical example of this class of polymer is ABS copolymer comprising a dispersed phase of butadiene, an intermediate phase of styrene-acrylonitrile grafted to the butadiene with a continuous phase SAN.[19,20]

Several factors control the morphology-toughness behavior: particle number density, particle size, particle nearest neighbor distance, matrix-particle adhesion strength, and physical-mechanical properties of the particles. These are in-turn controlled by the synthesis and processing conditions. Among them, the particle size and the size distribution appear to be the main parameters responsible for enhancing toughness.

Figure 9 shows clear distinguishable rounded rubber particles. A high magnification SEM image, shown in Figure 10, clearly shows the existence of two sizes of rubber particles from optical micrographs [Figure 10(a)] and from SEM pictures [Figure 10(b)] with the smaller diameters ranging from 10 nm to 200 nm and larger diameters ranging from 400 nm to 600 nm. Figure 10(b) shows grafted surface layer rubber particles illustrating a lot of graft boundaries and small white SAN.

Fractography was performed on the fatigue fracture surfaces of the ABS copolymer specimens using SEM to characterize the fatigue regimes: incubation, MSC, and LC growth and also quantify sizes of particles from which the fatigue cracks incubated. SEM analysis of fracture surfaces showed that debonded or fractured particles near the free surface had incubated fatigue cracks for the ABS copolymer specimens.

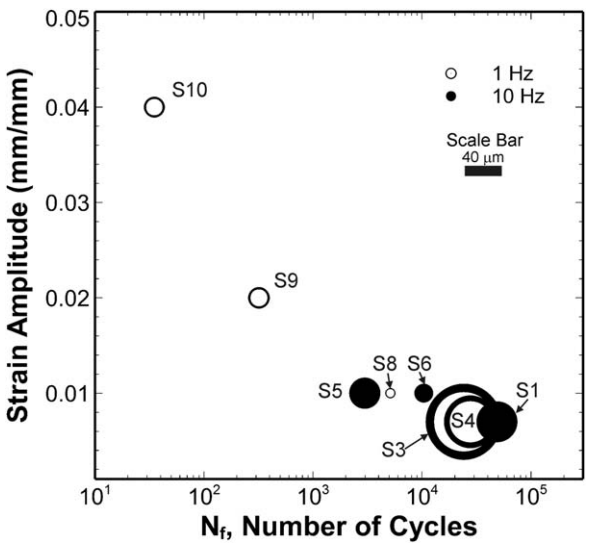


**Figure 13.** Strain amplitude versus cycles to failure for an acrylonitrile butadiene styrene copolymer showing that high cycle fatigue is more sensitive to large defects and equivalent strain rates for 1 Hz and 10 Hz.

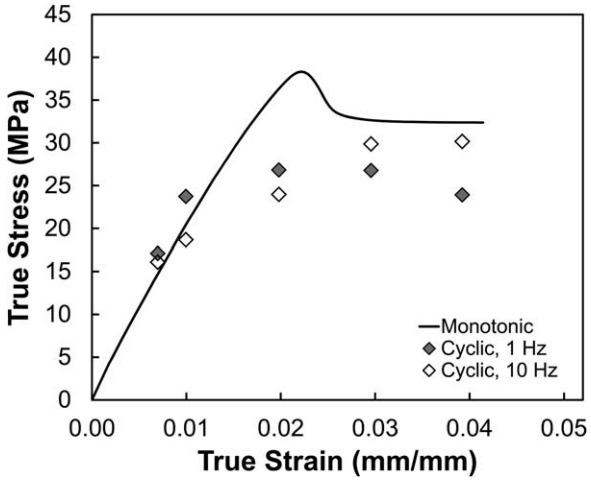


**Figure 14.** Monotonic tensile and cyclic stress versus strain behavior for fully reversed experiments at half lifetime for an acrylonitrile butadiene styrene copolymer.

A comparison of fracture surfaces for specimens performed at 0.007 and 0.01 strain amplitudes at both 1 Hz and 10 Hz, respectively, are shown in Figure 11. As the strain amplitude decreased, the fracture surface became smoother due to smaller crack growth increments. At higher frequencies, there is a higher equivalent strain rate observed and a slower crack growth rate also leading to a smoother fracture surface that follows observations by Ishikawa and Ogawa[21] for glassy polymers.

Simple observations of the fracture surface did not give clear distinctions for the three fatigue regimes; however, incubation can be estimated at 15% for the ABS copolymer due to the typical defect sizes responsible for incubating fatigue cracks and the nanoporosity contained within the material matrix.[3,10,22–24]

Furthermore, SEM was used to quantify the square root of the particle areas for particles from which fatigue cracks incubated for respective upper and lower bounds of fatigue life. The respective square root particle areas and number of cycles to failure are also shown for each specimen in Figure 12.

**Table II.** MSF Parameters and Material Properties for an Acrylonitrile Butadiene Styrene

| Property | Value |
|---|---|
| $C_n$ | 0.3 |
| $C_{INC}$ | 0.35 |
| $\alpha$ | −0.6 |
| $q$ | 2.35 |
| $y_1$ | 70 |
| $z$ | 1.1 |
| $r$ | 0.2 |
| $C_I$ | 12,500 |
| $C_{II}$ | 0.4 |
| $\chi$ | 0.32 |
| $\Delta CTD_{th}$ | 0.000425 |

Large inclusions with an approximate square root area between 46.47 $\mu$m and 66.97 $\mu$m, and fractured particles near the free surface ranging from 8.04 $\mu$m to 40.55 $\mu$m in equivalent square root area, were found to be the initiation sites on most ABS copolymer fracture surfaces. The larger inclusions found within the virgin matrix, previously shown in Figure 3, are comparable in size and shape to the inclusions in which fatigue cracks incubated for specimens fatigued at 0.007 strain amplitude at 1 Hz as shown in Figure 12 (specimens S3 and S4).

The effect of particle size on a strain-life fatigue plot is shown in Figure 13. In this graph, the circles represent the particle size and are drawn to scale. The visual representation where larger particles yielding lower fatigue lifetimes is shown where strain

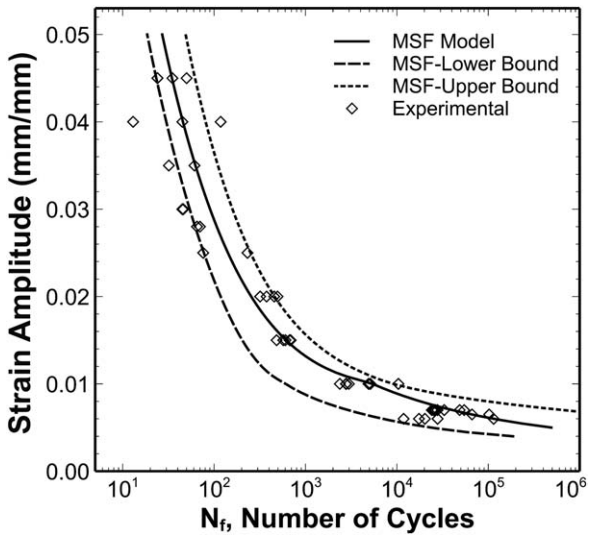


**Figure 15.** Multistage fatigue (MSF) total life correlation of experimental fatigue data shown with upper and lower bounds for the acrylonitrile butadiene styrene copolymer.

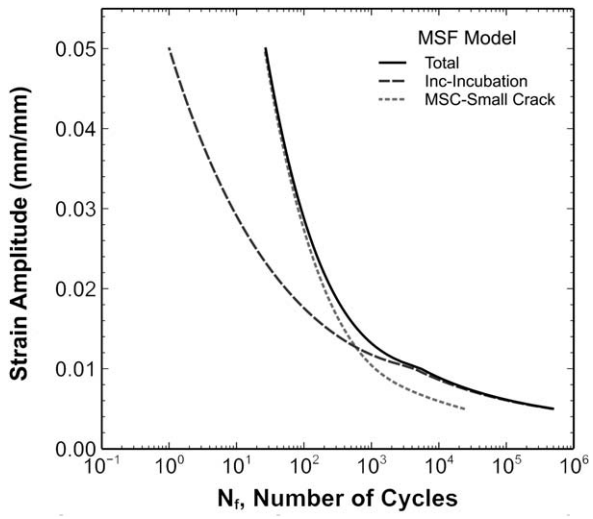


**Figure 16.** The multistage fatigue (MSF) model prediction for the breakdown of regimes of incubation and small crack growth for the acrylonitrile butadiene styrene (ABS) copolymer.

effects are shown to be more prevalent for the lower strain amplitude where larger defects were prone to initiate fatigue cracks.

Larger particles lead to lower fatigue lifetimes due to higher stress concentrations initiating fatigue cracks. In the LCF regime for the ABS copolymer, where the strain amplitude applied is greater than 0.01, the fatigue life appears to be less sensitive to particle size. This could be attributed to massive amounts of plasticity and deformation distributed throughout the material in the low cycle regime. In the high cycle regime, there appears to be more sensitivity to larger defects and frequency because the stress concentration becomes more localized.

## MULTISTAGE FATIGUE MODELING

### Multistage Fatigue Model

The MSF model has been used to quantify the microstructural effects on fatigue life for many metal alloys.[12,25–30] The model was originally developed by McDowell et al.[12] for a cast aluminum alloy. Its distinctive feature is the capability to predict the observed variability in fatigue with respect to the variation of microstructural properties such as second phase particle size, pore size, and porosity, among others. However, polymeric material models that incorporate microstructure properties into fatigue behavior are lacking in the literature. In this research, the MSF model is adapted for a thermoplastic material ABS.

The MSF model considers three stages of fatigue damage: INC, MSC growth, and LC growth. A brief summary of the MSF model is given below, further details and theoretical basis are found elsewhere.[12] The governing equations in the MSF model are listed below:

$$N_{\text{Total}} = N_{\text{INC}} + N_{\text{MSC}} + N_{\text{LC}} \tag{1}$$

$$C_{\text{INC}}\, N_{\text{INC}}^{\alpha} = \beta \tag{2}$$

$$\beta = \frac{\Delta\gamma_{\max}{}^{p*}}{2} = Y[\varepsilon_a - \varepsilon_{\text{th}}]^q, \qquad \frac{l}{D} < \eta_{\lim}, \tag{3}$$

$$\beta = \frac{\Delta\gamma_{\max}{}^{p*}}{2} = Y\left(1+\zeta\frac{l}{D}\right)[\varepsilon_a - \varepsilon_{\text{th}}]^q, \qquad \frac{l}{D} > \eta_{\lim}. \tag{4}$$

$$\frac{l}{D} = \eta_{\lim}\frac{\langle \varepsilon_a - \varepsilon_{\text{th}}\rangle}{\varepsilon_{\text{per}} - \varepsilon_{\text{th}}}, \qquad \frac{l}{D} \le \eta_{\lim}, \tag{5}$$

$$\frac{l}{D} = 1-(1-\eta_{\lim})\left(\frac{\varepsilon_{\text{per}}}{\varepsilon_a}\right)^r, \qquad \frac{l}{D} > \eta_{\lim}, \tag{6}$$

$$\left(\frac{da}{dN}\right)_{\text{MSC}} = \chi(\Delta\text{CTD} - \Delta\text{CTD}_{\text{th}}), \qquad a_i = 0.625D \tag{7}$$

$$\begin{aligned}\Delta\text{CTD} = {} & C_{II}\left(\frac{GS}{GS_0}\right)^{\omega}\left(\frac{GO}{GO_0}\right)^{\xi}\left[\frac{U\Delta\hat{\sigma}}{S_{\text{ut}}}\right]^{\zeta} a_i \\ & + C_I\left(\frac{GS}{GS_0}\right)^{\omega'}\left(\frac{GO}{GO_0}\right)^{\xi'}\left(\frac{\Delta\gamma^{\text{P}}_{\max}}{2}\right)^2\end{aligned} \tag{8}$$

The total fatigue life is given by eq. (1), where $N_{\text{INC}}$ is the number of cycles to incubate a crack. $N_{\text{MSC}}$ is the number of cycles required for propagation of a microstructurally small crack, and $N_{\text{LC}}$ is the number of cycles required for long crack propagation. In this research, we focus mainly on the incubation and MSC regimes as others have focused on the long crack behavior.

Crack incubation involves nucleation plus small crack growth around of an inclusion on the order of $\frac{1}{2}$ $D$ ($a_i$), where $D$ is the inclusion particle diameter or pore size. The MSC regime includes lengths where $a_i < a < k$ microstructural (MS), with MS defined as a characteristic length scale of interaction with MS features, and $k$ as a multiplier in the range between one and three.

Equation (2) is used to model fatigue damage incubation life, and is based on a modified Coffin-Manson law. $C_{\text{INC}}$ and $\alpha$ are linear and exponential material constants selected to be that of the macroscopic Coffin-Mason law.[12] The nonlocal damage parameter, $\beta$, is the maximum plastic shear strain amplitude located around the particle or defect and depends on ratio of the plastic zone to the particle or defect size ($l/D$). The parameters $\varepsilon_{\text{th}}$, $\varepsilon_{\text{per}}$, $\eta_{\lim}$, $r$, and $q$ describe the ratio of plastic zone to the particle size or defect as a function of the strain amplitude ($\varepsilon_a$). The parameter $Y$ is correlated as $Y = y_1 + (1+R)y_2$, where $R$ is the load ratio, and $y_1$ and $y_2$ are model constants. For completely reversed loading cases, $Y = y_1$.

Crack growth in the MSC stage is governed by the range of the crack tip displacement, ΔCTD, which is proportional to the crack length, and the $n$th power of the applied stress amplitude, $\sigma^n{}_a$, in the HCF regime and to the macroscopic plastic shear strain range in the LCF as given by eq. (7). Where $\chi$ is a material constant and $\Delta\text{CTD}_{\text{th}}$ is the threshold for crack tip displacement. The crack tip displacement is a function of the remote loading [eq. (8)], and $C_{\text{I}}$ , $C_{\text{II}}$ , and $\zeta$ are material dependent parameters which capture the microstructural effects on MSC growth.

Microstructural features admitted into the MSF model, but not limited to, are the following: grains, dendrite cell size, nearest neighbor distance, porosity, and size of inclusions (particles and voids). Moreover, polymers are more susceptible to thermo-mechano-chemical degradation when compared with most metals. The components of ABS are poor thermal conductors that lead to a hysteresis heating and reducing the modulus of the material. Furthermore, the material is sensitive to microstructural feature variability, processing, frequency, and temperature effects. Due to the high sensitivity that these effects have on polymers, polymeric materials are generally considered much more complex in comparison to most metal alloys; however, there are some similarities which can reduce the gap between the two material families.

### MSF Model Correlation

In order to apply the MSF model to the ABS material, various parameters and constant materials were computed. As mentioned previously, the model consists of three stages, with each stage being driven by different parameters. Below are explained the parameters that have been used to model the polymeric material.

The monotonic stress strain behavior was compared with the cyclic stress–strain behavior as shown in Figure 14. The maximum tensile stress of stabilized hysteresis loops at respective

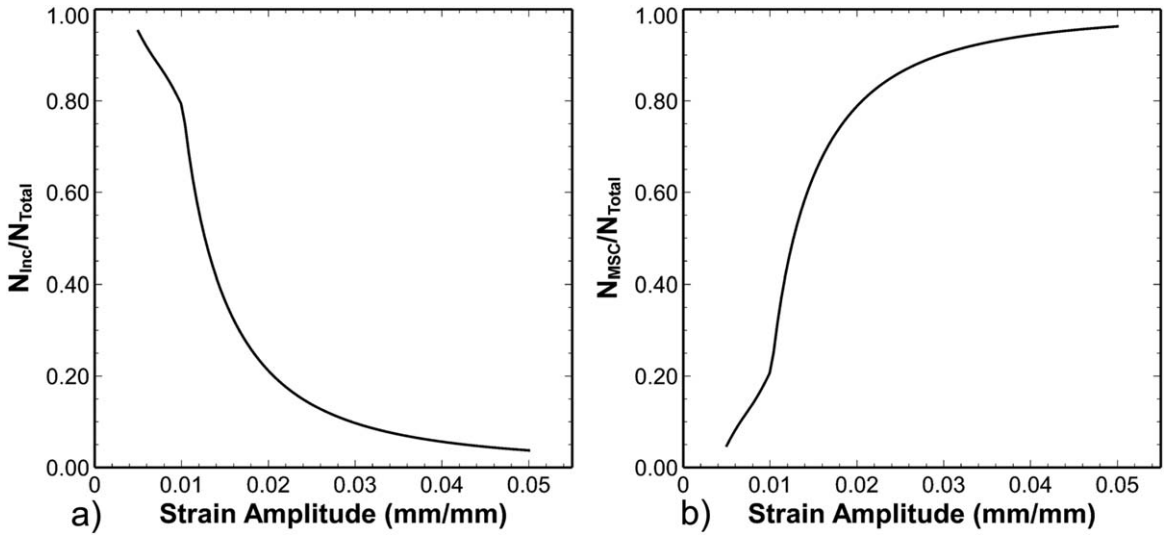


**Figure 17.** (a) Incubation life ($N_{INC}$) as a fraction of total fraction life, and (b) microstructurally small crack growth ($N_{MSC}$) life as a fraction of total fraction life against strain amplitude derived from multistage fatigue (MSF) model predictions.

strain amplitudes was plotted for the cyclic stress–strain curve to obtain the cyclic strength coefficient and hardening exponent for the ABS copolymer following Bannantine et al.[31]

The first stage, INC is mainly dominated by the microstructural features serving as stress concentrators. Among these, features are found all types of defects in a material, such as pores, inclusions, second phase particles, etc. Various MSF parameters for this stage are determined by finite element simulations and have been previously determined.[24] The primary microstructure–property used to model this regime was the average particle size for INC.

The small crack growth regime is dictated by the microstructural properties at the next length scale order of magnitude as explained in a previous section. Equations (7) and (8) determine the behavior of this region. The crack growth rate given by eq. (7) obeys a power law affected by a constant of proportionality. The constant $\chi$ was determined as $\sigma_e/\sigma_{ut}$ following,[32] and the crack tip displacement threshold, $\Delta CTD_{th}$ which is generally assigned a value on the order of the Burger's vector for metal alloys, was taken as the magnitude of the shear displacement of the sheared region of an amorphous polymer.[33]

Equation (8) represents the contributions of high cycle and LCF regimes to crack growth propagation. Although eq. (8) involves properties such as grain size (GS) and grain orientation (GO) typical of metals, the real function of this equation is to capture the properties that affect the behavior of the small crack stage. Accordingly, the quotients $GS/GS_0$ and $GO/GO_0$ in eq. (8) are factors representing the properties involved in the crack growth behavior, and they were set to unity in this study. Therefore, the equation was simplified as follows

$$\Delta CTD = C_{II}\left[\frac{U\Delta\hat{\sigma}}{S_{ut}}\right]^{\zeta} a_i + C_I\left(\frac{\Delta\gamma^P_{max}}{2}\right)^2 \quad (9)$$

The LC growth regime of the MSF model has historically followed classical linear elastic fracture mechanics approaches[24,28]; however, the modeling approach presented in this study is focused on incubation and MSC regimes of the ABS copolymer.

Figure 15 shows the correlations of the MSF model to the experimental strain-life data. Table II provides a summary of the model constants used to correlate the MSF to fully reversed uniaxial strain life results for the ABS alloy. As shown in Figure 15, the MSF model predictions are in good agreement to the experimental results. Error bands can be built for the MSF model based on the distribution of microstructural features. Here for illustration purposes is shown in Figure 15 lower and upper limits of the MSF model. These bands were constructed using a maximum particle size of 190 $\mu$m and a minimum particle size of 5 $\mu$m, respectively, for the fatigue fracture surface and responsible for the incubation of cracks.

To explore the contributions to the total life by the incubation and MSC growth stages, a breakdown of the lives for the MSF model predictions for incubation and MSC growth are shown in Figure 16. The relative influence of incubation compared with MSC growth to the total life is small when the applied strain is large. However, when the applied strain is small, then the relative influence of incubation compared with the MSC growth is greater. This increase continues to a level where incubation becomes dominant as the applied strain becomes much less.

In an effort to quantify the contributions of the incubation and MSC stages considered in the MSF model, two graphs are shown in Figure 17. Figure 14(a) shows the ratio of incubation life to the total life ($N_{INC}/N_T$). It is clear from Figure 17 that for strain amplitudes equal and lower than 0.01, the incubation life represents 80% or more.

## CONCLUSIONS

Cyclic fatigue behavior for a thermoplastic ABS copolymer was quantified with microstructural properties that govern the uncertainty of the mechanical response. A MSF model was used

to capture these microstructural features and effects on strain-life fatigue behavior. The following conclusions and recommendations were generated as a result of this study.

- Energy-dispersive X-ray spectroscopy results show that the defects responsible for incubation of fatigue cracks are primarily composed of carbon, which can be attributed to polybutadiene. In addition, trace amounts of nitrogen on some defects show some acrylonitrile is possibly present. Similar findings for the composition of defects in ABS copolymers using a Raman imaging technique was found in work by Marrisen et al.[15]
- Although no engineering material like the ABS copolymer has been correlated to the MSF model where particle was softer than the matrix before this work, clearly the MSF model would admit such a material, based on studies by Gall et al.[34] Up to this point, the MSF model had only been applied to metal alloys, where in general the particle is harder than the matrix.
- Fatigue cracks for the 0.01 strain amplitude and lower tests were found to incubate at particles on or near the free surface of the cylindrical fatigue specimens. Fracture surfaces for strain amplitudes of 0.015 to 0.02 show a similar distributed faceting on fracture surfaces as observed in studies performed by Marissen et al.[15] Fatigue specimens performed at 0.025 to 0.035 strain amplitudes show quick decreases in peak tensile stress versus the number of cycles. For these specimens, the fracture surfaces are difficult to observe anything due to the massive thermo-mechanical degradation.
- As the particle size increases, the number of cycles to failure decreases following similar work of metal alloys[30,35]; hence, the debonding of particles has a similar effect on the fatigue lifetime independent of the material (metal or polymer) observed.
- Tests performed at higher frequencies led to higher fatigue lifetimes, which could be attributed to the thermal softening of the polymer in which the stress was relieved thus changing the failure mechanism from lower frequency mechanisms such as crazing or shear banding.

Further investigation into degradation mechanisms including crazing and shear banding need to be performed for possible inclusion in MSF modeling of polymers as possible texture effects. The texture effects for polymers were not introduced in this work and future work and extension of the MSF should include an "evolving" texture for polymers. Furthermore, studies on the competing influence of frequency and temperature effects due to environmental subjection or generation is needed, as the current MSF model does not explicitly include these effects.

## ACKNOWLEDGMENTS

This work was supported by the US Army TACOM Life Cycle Command under Contract No. W56HZV-08-C-0236. Any opinions, findings, and conclusions or recommendations expressed in this writing are those of the authors and do not necessarily reflect the views of the US Army TACOM Life Cycle Command.

## REFERENCES

1. Rabinowitz, S.; Krause, A. R.; Beardmore P. *J. Mater. Sci.* **1973**, *8*, 11.
2. Rabinowitz, S.; Beardmore, P. *J. Mater. Sci.* **1974**, *9*, 81.
3. Radon, J. C. *Int. J. Fract.* **1980**, *16*, 533.
4. Hertzberg, R. W.; Nordberg, H.; Manson, J. A. *J. Mater. Sci.* **1970**, *5*, 521.
5. Hertzberg, R. W.; Manson, J. A. In Fatigue of Engineering Plastics; Academic Press: New York, **1980**.
6. Schinker, M. G.; Konczol, L.; Doll, W. *Colloid Polym. Sci.* **1984**, *262*, 230.
7. Konczol, L.; Doll, W.; Bevan, L. *Colloid Polym. Sci.* **1990**, *268*, 814.
8. Adams, M. E.; Buckley, D. J.; Colborn, R. E.; England, W. P.; Schissel, D. N. Rapra Review Report 70 Review Report; RAPRA Technology Ltd.: UK, **1993**.
9. Van der Giessen, E.; Estevez, R.; Pijnenburg, K. G. W.; Tijssens, M. G. A. In European Conference on Computational Mechanics (ECCM' 99), Munchen, Germany, **1999**.
10. Maiti, S.; Geubelle, P. H. *Eng. Fract. Mech.* **2005**, *72*, 691.
11. Chen, C. C.; Chheda, N.; Sauer, J. A. *J. Macromol. Sci. Phys.* **1981**, *B19*, 565.
12. McDowell, D. L.; Gall, K.; Horstemeyer, M. F.; Fan, J. *Eng. Fract. Mech.* **2003**, *70*, 49.
13. Suresh, S. Fatigue of Materials, 2nd ed.; Cambridge University Press: Cambridge, **2003**.
14. Zaroulis, J. S.; Boyce, M. C. *Polymer* **1997**, *38*, 1303.
15. Marissen, R.; Schudy, D.; Kemp, A. V. J. M.; Coolen, S. M. H.; Duijzings, W. G.; Van der Pol, A.; Van Gulick, A. J. *J. Mater. Sci.* **2001**, *36*, 4167.
16. Arruda, E. M.; Boyce, M. C.; Jayachandran, R. *Mech. Mater.* **1995**, *19*, 193.
17. Sauer, J. A.; Richardson, G. C. *Int. J. Fract.* **1980**, *16*, 499.
18. Felton, L. A. *AAPS PharmSciTech* **2007**, 8, Article 112.
19. Riew, C. K.; Kinloch, A. J. Toughened Plastic I, Advances in Chemistry Series, 233; American Chemical Society: Washington, DC, **1993**.
20. Bucknall, C. B.; Reddock, S. E. *J. Mater. Sci.* **1985**, *20*, 1434.
21. Ishikawa, M.; Ogawa, H. *J. Macromol. Sci. Phys.* **1981**, *B19*, 421.
22. McEvily, A. J.; Boettner, R. C.; Johnston, T. L. In Proceedings of the 10th Sagamore AMR Conference, Syracuse, **1964**; p 95.
23. Weiland, H.; Nardiello, J.; Zaefferer, S.; Cheong, S.; Papzian, J.; Raabe, D. *Eng. Fract. Mech.* **2009**, *76*, 709.
24. Xue, Y.; McDowell, D. L.; Horstemeyer, M. F.; Dale, M. H.; Jordon, J. B. *Eng. Fract. Mech.* **2007**, *74*, 2810.
25. Horstemeyer, M. F.; Yang, N.; Gall, K. A.; McDowell, D. L.; Fan, J.; Gullett, P. *Acta Mater.* **2004**, *52*, 1327.
26. El Kadiri, H.; Xue, Y.; Horstemeyer, M. F.; Jordon, J. B.; Wang, P. T. *Acta Mater.* **2006**, *54*, 5061.
27. Xue, Y.; Horstemeyer, M. F.; McDowell, D. L.; El Kadiri, H.; Fan, J. *Int. J. Fatigue* **2007**, *29*, 666.
28. Jordon, J. B.; Horstemeyer, M. F.; Yang, N.; Major, J. F.; Gall, K.; Fan, J.; McDowell, D. L. *Metall. Mater. Trans. A* **2009**, *41*, 356.

29. Xue, Y.; Pascu, A.; Horstemeyer, M. F.; Wang, L.; Wang, P. T. *Acta Mater.* **2010**, *58*, 4029.

30. Jordon, J. B.; Gibson, J.; Horstemeyer, M. F.; El Kadiri, H.; Baird, J.; Luo, A. A. *Mater. Sci. Eng. A* **2011**, *528*, 6860.

31. Bannantine, J. A.; Comer, J. J.; Handrock, J. L. In Fundamentals of Metal Fatigue Analysis; Prentice Hall, Inc.: Englewood Cliffs, New Jersey, **1990**; Chapter *2*, pp 40–87.

32. McClintock, F. A. In Engineering Against, Fatigue Proceedings of an International Conference; Beynon, J. H., Brown, M. W., Lindley, T. C., Smith, R. A., Tomkins, B., Eds.; Taylor & Francis, Inc: UK, **1997**; 17–21 March, Chapter *24*, pp 227–241.

33. Bowden, P. B.; Raha, S. *Philos. Mag.* **1974**, *29*, 149.

34. Gall, K.; Horstemeyer, M. F.; McDowell, D. L.; Fan, J. *Mech. Mater.* **2000**, *32*, 277.

35. Bernard, J. D.; Jordon, J. B.; Horstemeyer, M. F.; El Kadiri, H.; Baird, J.; Lamb, D.; Luo, A. A. *Scr. Mater.* **2010**, *63*, 751.